Published in IET Electric Power Applications
Received on 29th August 2007
Revised on 4th January 2008
doi: 10.1049/iet-epa:20070372

ISSN 1751-8660

Analytical closed-form investigation of PWM inverter induction motor drive performance under DC bus voltage pulsation

J. Klima[1] *M. Chomat*[2] *L. Schreier*[2]

[1]*Department of Electrical Engineering and Automation, CZU, 6 Suchdol, Prague 16521, Czech Republic*
[2]*Department of Electrical Engineering, Institute of Thermomechanics, Academy of Sciences of the Czech Republic, Prague 182 020, Czech Republic*
E-mail: klima@tf.czu.cz

Abstract: The voltage unbalance conditions at the input rectifier stage of the AC–DC–AC rectifier-inverter fed induction motor drive is analysed. This unbalance can cause significant voltage harmonic of twice the line frequency $2f_1$ in the DC bus. This voltage ripple can have a degrading effect on the induction-machine performance characteristics. The authors present an analytical closed-form mathematical model and analysis of the impact of DC bus ripple voltage of the three-phase voltage source inverter with the space-vector PWM on the induction machine phase voltages, currents and torque pulsations. The analytical expressions for the voltage and current space vectors as a function of the DC bus voltage pulsation are derived. Using superposition, the separate parts of the motor currents can be determined. From the current space vectors, the torque behaviour is estimated, again as a function of DC link voltage pulsation. Next, it is shown that the DC link voltage ripple components may cause large torque pulsation. The proposed analytical method is based on the mixed p–z approach, enabling presentation of the results in lucid and closed form. To verify the effectiveness of the proposed analytical model, experimental results based on laboratory setup were obtained.

1 Introduction

In most industrial applications, the induction machine is supplied by a voltage source inverter (VSI). The inverter experiences, in some situations, a substantial ripple of the DC bus voltage that may negatively affect the supply of the connected electric machines. Input voltage unbalance and/or sag conditions can have serious performance consequences in induction motors. As it was shown [1], the unbalance conditions in the three-phase input line voltages may cause the rectifier stage to enter a single-phase rectifier operation. This situation can create significant voltage harmonic in the DC bus at twice the line frequency (100 Hz for 50 Hz supply.)

This DC bus voltage ripple affects the PWM output voltage waveforms, causing low-frequency harmonic currents to flow into the motor.

An increase in electric losses, excessive rise of the motor temperature, appearance of the torque pulsation and noise problems as well as the DC bus capacitor stress are just some of the possible problems [2, 3]. So, the analysis of the DC link voltage pulsation and its influence on the motor performances is of great importance.

The DC bus voltage pulsation is composed of several sources as follows [4].

(a) The diode rectification of the AC line voltage causes pulsation components [1].

(b) Unbalance in the AC power supply generates 100 or 120 Hz component [4].

(c) In some faulty conditions in the front-end rectifier, DC link voltage may again consist of pulsation [5].

(d) Transient voltage sags in the three-phase input line voltages can cause the rectifier stage to enter single-phase rectifier operation with corresponding DC bus voltage pulsation [6].

The mathematical model providing closed-form expressions to estimate the machine currents and torque waveforms as a consequence of DC link voltage ripple was presented in [1]. The analysis is simplified by the assumption that the inverter PWM voltage is approximated only by the fundamental harmonic. It was derived that the dominant frequency component that appears in the DC link voltage during the single-phase operation mode oscillates at twice the supply angular frequency ($2\omega_1$), and as a result, [1, equation (7)], the DC bus voltage can be approximated by the constant value V_{dc} and the pulsation part

$$V_{DC2}\cos(2\omega_1 t + \theta_2),$$

where V_{DC2} is the amplitude of the second-harmonic voltage component and θ_2 the corresponding phase angle.

This paper presents a mathematical model which enables us to solve both the steady-state and transient-state performance of the three-phase VSI under DC link voltage ripple feeding an induction motor and respecting the real PWM inverter voltage. The analytical closed-form solution makes use of the Laplace and modified Z-transforms of the space vectors (mixed p–z approach [7, 8]). From the Laplace transform of the stator voltage vectors, we can also derive the Fourier series to predict the voltage harmonic spectra.

The analysis is made under the assumption that the motor runs at a constant speed. The electromechanical time constant is much larger than the electrical ones, and therefore it is reasonable to assume that the rotor speed remains constant during a sampling period.

The attention is focused on the calculation of the closed-form expressions for the stator and rotor currents. From these equations, an analytical expression for the electromagnetic torque in dependence of the DC link pulsation is derived. Torque ripple deteriorates the static and dynamic characteristics of induction motors and it may become an important issue in induction motor design. It may cause mechanical oscillations, which are particularly dangerous in resonant frequencies of the load. Moreover, torque ripple leads to an increase in the motor noise. Particularly, the appearance of the sixth torque harmonic was observed by many researchers [9, 10]. But in this paper, it will be shown that the DC link ripple voltage components may give rise to an additional large torque ripple component.

The paper contributes to a better understanding of the effects of DC link voltage ripple conditions on operation of an induction machine by providing closed-form expressions both in time and frequency domain, taking into account the real PWM waveforms. In particular, this mathematical model provides a useful tool for the development of the DC link ripple mitigation technique by a proper modulation technique of the inverter.

The proposed mathematical model has also been verified by experiment. The experiments were provided both in six-step and space-vector PWM (SVPWM) regimes. The experimental results show good agreement with the theoretical prediction.

2 Stator voltage space vectors

A simplified scheme of the system is shown in Fig. 1. Three-phase AC line voltages are fed to a three-phase rectifier bridge. The DC bus voltage $V_{DC}(t)$ is buffered by the two DC bus capacitances C. The output part is composed of the PWM inverter consisting of six IGBT switches and their antiparallel diodes. The PWM voltage waveforms are delivered to the induction machine following a constant volts-per-hertz algorithm.

This paper is focused primarily with the output part of the drive. This approach takes into account the DC link voltage ripple, due to the finite DC link capacitors. It has been shown [1] that the input rectifier stage of the system shown in Fig. 1 can easily slip into single-phase operation during the input line voltage sag or/and unbalance conditions. The dominant AC component in the DC bus voltage ripple occurs at the second line harmonic frequency (100 Hz).

We assume that the DC link voltage contains both the constant and pulsation parts that may be expressed as

$$V_{DC}(t) = V_{DC0} + \sum_{i=1}^{\infty} \Delta V_{DCi}\ \cos(i2\omega_1 t + \psi_i) \qquad (1a)$$

The voltage ripple appearing across the DC link capacitor terminals contains, only even-order harmonics [5]. The dominant AC frequency component that appears in the DC link voltage pulsates at twice the excitation frequency ($2f_1$).

As a result for the closed-form mathematical solution, we suppose as in [1] that the DC link voltage can be approximated by the constant average value V_{DC} and pulsation part $\Delta\ V_{DC1}\ \cos\ 2\omega_1 t$, where ω_1 is an angular frequency of the supply voltage ($2\pi\ 50$ or $2\pi\ 60$, s^{-1}).

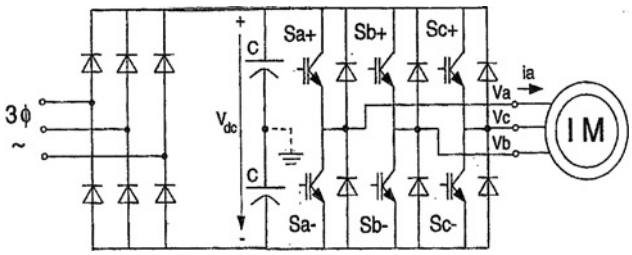

Figure 1 *Rectifier-inverter induction motor drive*

doi: 10.1049/iet-epa:20070372

But if needed we can take into consideration from (1a) also the next higher harmonics with the angular frequency $i2\omega_1$, $i = 2, 3, 4, \ldots$. As it will be shown latter, based on the principle of superposition in case of taking into account more higher harmonics, we obtain for each harmonic the two additional terms: a positive sequence term with angular frequency $i2\omega_1$ and a negative sequence term with angular sequence $-i2\omega_1$.

The switching elements will be considered as ideal switches. We also assume constant rotor speed and linear parameters of the motor.

As the dominant AC component in the resulting DC bus voltage $V_{DC}(t)$ is created by the second-harmonic voltage component, it also dominates in generation of undesirable effects in the induction-machine operating performance characteristics. Next, attention is focused on developing the closed-form mathematical model that quantifies the induction-machine performance effects caused by this second-harmonic voltage component.

The stator voltage space vector can be expressed in the complex $\alpha\beta$ plane with respect to $\pi/3$ symmetry as follows

$$V(n, \varepsilon) = (V_{DC} + \Delta V_{DC}) \cos \frac{(2 \cdot \omega_1(n+\varepsilon)T)2}{3} e^{j\omega_0 T \cdot n} \tag{1b}$$

where $\omega_0 = 2\pi/T_0$ is the inverter output fundamental angular frequency.

In (1b), time is expressed in per units as

$$t = (n+\varepsilon)T = \frac{(n+\varepsilon)T_0}{6} \tag{2}$$

where $T = T_0/6$ is a sector period, n is a number of a sector and ε is a per-unit time inside sector T.

$$0 \le \varepsilon \le 1 \tag{2a}$$

To express the voltage space vector with SVPWM, we must include in (1b) also the modulation function, and the stator voltage vector is calculated as follows

$$\begin{aligned} V(n, \varepsilon) &= \frac{[V_{DC} + \Delta V_{DC} \cos 2\omega_1(n+\varepsilon)T]}{3} 2e^{jn(\pi/3)} \\ &\quad \times \sum_k f(\varepsilon, k) e^{j\pi(\alpha_k/3)} \\ &= \frac{2}{3} V_{DC} e^{jn(\pi/3)} \sum_k f(\varepsilon, k) e^{j\pi(\alpha_k/3)} \\ &\quad + \frac{2}{3} \Delta V_{DC} \cos[2\omega_1(n+\varepsilon)T] e^{jn(\pi/3)} \sum_k f(\varepsilon, k) \\ &\quad \times e^{j\pi(\alpha_k/3)} \\ &= V_d(n, \varepsilon) + V_p(n, \varepsilon) \end{aligned} \tag{3}$$

In (3), $V_d(n, \varepsilon)$ is the voltage space vector created from the smooth part of the DC bus voltage (V_{DC}), $V_p(n, \varepsilon)$ is the voltage space vector caused by the second-harmonic voltage component (ΔV_{dc}) and $\Sigma_k f(\varepsilon, k).e^{j\pi/3.\alpha_k}$ is the modulation function given by the switching instants within the kth pulse. This function contains both time and phase vector dependency.

Time dependency is given as follows

$$\begin{aligned} &f(\varepsilon, k) = 1, \quad \text{for} \quad \varepsilon_{k\mathrm{A}} \le \varepsilon \le \varepsilon_{k\mathrm{B}}, \\ &f(\varepsilon, k) = 0 \text{ else} \end{aligned} \tag{3a}$$

where $\varepsilon_{k\mathrm{A}}$ is the start point setting per unit time of the kth pulse and $\varepsilon_{k\mathrm{B}}$ the end point setting per unit time of the kth pulse. The duty ratio switching time is

$$\Delta\varepsilon_k = \varepsilon_{k\mathrm{B}} - \varepsilon_{k\mathrm{B}} \tag{3b}$$

The expressions for the switching times in the normal SVPWM are given as follows

$$\begin{aligned} \Delta\varepsilon_1 &= \frac{\Delta T_1}{T} = \frac{m_{id}}{N_1} \sin(60^\circ - \rho) \\ \Delta\varepsilon_2 &= \frac{\Delta T_2}{T} = \frac{m_{id}}{N_1} \sin\rho \\ \Delta\varepsilon_0 &= \frac{1}{N_1} - \Delta\varepsilon_1 - \Delta\varepsilon_2 \end{aligned} \tag{3c}$$

where

$$m_{id} = \frac{\sqrt{3}}{V_{DC}} V_{AV}, \quad N_1 = \frac{T}{\Delta T}$$

m_{id} is a modulation factor, V_{AV} is the reference voltage, T is a sector period, ΔT is a switching period and ρ is a polar angle of the reference voltage vector referring to real axis.

Phase dependency is given by the function

$$g(k) = e^{j\pi/3\alpha_k} \tag{3d}$$

where α_k shows which voltage vector is used in the kth pulse.

For the conventional SVPWM where two adjacent space vectors within a sampling period are used, α_k can be 0 or 1 (i.e. voltage vectors in nth sector period can have direction $e^{j(\pi/3)n} e^{j(\pi/3)0} = e^{j(\pi/3)n}$ and $e^{j(\pi/3)n} e^{j(\pi/3)1} = e^{j(\pi/3)(n+1)}$)

In the first sector during the first two sampling periods, the following voltage vector sequence is used: ($\boldsymbol{V}_0$-$\boldsymbol{V}_1$-$\boldsymbol{V}_2$-$\boldsymbol{V}_7$), ($\boldsymbol{V}_7$-$\boldsymbol{V}_2$-$\boldsymbol{V}_1$-$\boldsymbol{V}_0$), where $\boldsymbol{V}_0$ and $\boldsymbol{V}_7$ are the zero voltage vectors.

With regard to the voltage vector sequences within the first switching period (the two sampling periods), we can define

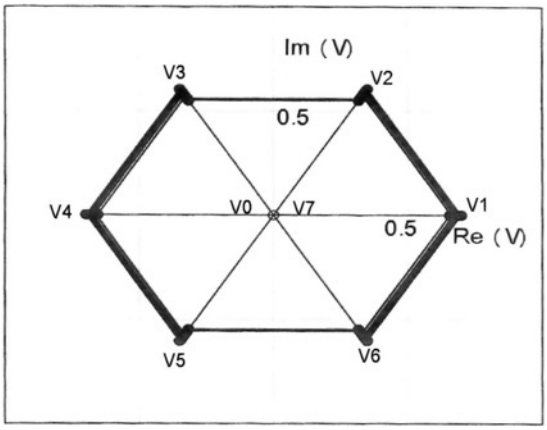

Figure 2 *Voltage space vector trajectory with DC-link pulsation component $\Delta V_{DC} = 0.05$*

α_k as follows

$$\alpha_{2m-1} = \frac{1+(-1)^m}{2}, \quad \alpha_{2m} = \frac{1+(-1)^{m+1}}{2} \tag{3e}$$

m is the number of sampling period.

The trajectory of $V(n, \varepsilon)$ in the complex $\alpha\beta$ plane for $\Delta V_{DC} = 0.05$ and $f_0 = f_1 = 50$ Hz, $f_{sw} = 3000$ Hz is shown in Fig. 2

As can be seen from Fig. 2, there are eight states available for this vector according to eight switching positions of the inverter in the $\alpha\beta$ complex plane (six non-zero vectors V_1–V_6 and two zero vectors V_0 and V_7). Comparing with the well-known trajectory of the voltage vectors with constant DC bus voltage, we can see the influence of the DC link pulsation component [time-dependent part of (3)].The pulsation part of the voltage space vectors separated into two parts [the positive and negative parts] is shown in Fig. 3.

Using the well-known formula for cosine function

$$\cos\ x = \frac{e^{jx} + e^{-jx}}{2} \tag{4}$$

we can write for the pulsating part in (3)

$$\begin{aligned} V_p(n, \varepsilon) &= \frac{\Delta V_{DC}}{3} e^{j2\omega_1 T(n+\varepsilon)} e^{jn\pi/3} \sum_k f(\varepsilon, k) e^{j\pi\alpha_k/3} \\ &\quad + \frac{\Delta V_{DC}}{3} e^{-j2\omega_1 T(n+\varepsilon)} e^{jn\pi/3} \sum_k f(\varepsilon, k) e^{j\pi\alpha_k/3} \\ &= V_{pp}(n, \varepsilon) + V_{pn}(n, \varepsilon) \end{aligned} \tag{5}$$

From (5), it may be seen that the pulsation part of the voltage space vector V_p (n, ε) may be resolved into two components: the positive sequence V_{pp} (n, ε) and the negative sequence V_{pn} (n, ε).

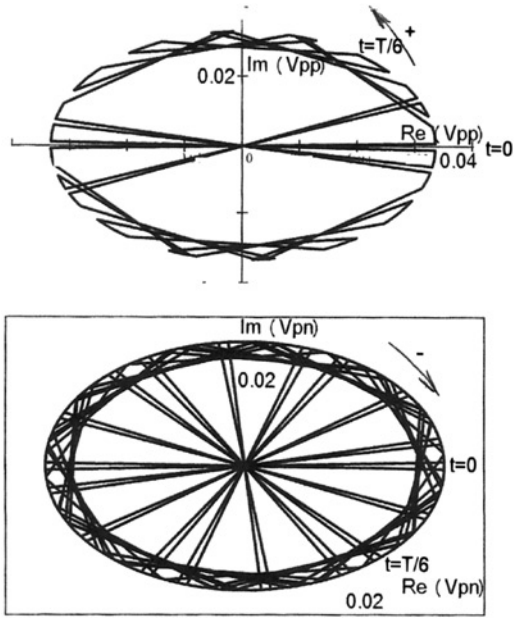

Figure 3 *Trajectories of two parts creating voltage space vector with DC link pulsation component $\Delta V_{DC} = 0.05$*

The trajectories of both parts in the complex plane for the same operating conditions as used to calculate trajectory in Fig. 2, are shown in Fig. 3.

3 Closed-form analytical model

3.1 Induction-machine circuit analysis

Using the mixed p–z approach as shown in [7, 8], we can derive the closed-form analytical expressions for the stator and/or rotor currents and also for the electromagnetic torque.

From these relations, we can estimate the influence of the DC link voltage pulsation on the currents and electromagnetic torque waveforms.

First, we can derive the Laplace transform of the symmetrical voltage vector sequences (3). For this, we can use the relation between the Laplace and modified Z-transforms [8].

Using (2) and its derivation $dt = T\,d\epsilon$, we can derive the Laplace transforms of the periodic waveform as

$$\begin{aligned} V(p) &= \sum_{n=0}^{\infty} \left(\int_0^1 V(n, \varepsilon) e^{-p(n+\varepsilon)T} T\ d\varepsilon \right) \\ &= T \int_0^1 V(z, \varepsilon) e^{-pT\varepsilon} d\varepsilon \end{aligned} \tag{6}$$

doi: 10.1049/iet-epa:20070372

where $z = e^{pT}$, and

$$V(z, \varepsilon) = \sum_{n=0}^{\infty} V(n, \varepsilon) z^{-n} \tag{7}$$

$V(z, \varepsilon)$ is the modified Z-transform of $V(n, \varepsilon)$.

Substituting (3) into (6) using the Z-transform of exponential functions, we can find the Laplace transform of the stator voltage vector as follows

$$\begin{aligned} \boldsymbol{V}_1(p) = {} & \frac{2}{3} V_{DC} \frac{1}{p} \frac{e^{pT}}{e^{pT} - e^{j\pi/3}} \sum_k (e^{-pT\varepsilon_{kA}} - e^{-pT\varepsilon_{kB}}) \\ & + \frac{1}{3} \Delta V_{DC} \frac{1}{p - 2j\omega_1} \frac{e^{pT}}{e^{pT} - e^{j(\pi/3 + 2\omega_1 T)}} \\ & \times \sum_k (e^{-T\varepsilon_{kA}(p - 2j\omega_0)} - e^{-T\varepsilon_{kB}(p - 2j\omega_0)}) \\ & + \frac{1}{3} \Delta V_{DC} \frac{1}{p + 2j\omega_1} \frac{e^{pT}}{e^{pT} - e^{j(\pi/3 - 2\omega_1 T)}} \\ & \times \sum_k (e^{-T\varepsilon_{kA}(p + 2j\omega_0)} - e^{-T\varepsilon_{kB}(p + 2j\omega_0)}) \\ = {} & \boldsymbol{V}_0(p) + V_{1P}(p - 2j\omega_1) + V_{1N}(p + 2j\omega_1) \end{aligned} \tag{8}$$

Equation (8) is the Laplace transform of the stator voltage vector, with respect to the influence of the DC link voltage ripple. It contains three parts. The first term is the Laplace transform of the stator voltage vector with constant value in the DC link voltage. The last two terms are the Laplace transform of the positive and the negative ripple components of the DC link voltage.

When we know the Laplace transform of the stator voltage vectors, we can derive the Laplace transform of the motor current vectors. In order to calculate the motor current space vectors, it is convenient to carry out the analysis in the stator reference frame.

From the motor equations in the stator reference frame, we can derive the Laplace transform of the stator and rotor currents, respectively, as follows

$$\begin{aligned} I_S(p) &= \boldsymbol{V}_1(p) \frac{A_S(p)}{B_S(p)} = \boldsymbol{V}_1(p) \frac{k_R + p - j\omega}{\sigma L_S (p - p_1)(p - p_2)} \\ I_R(p) &= \boldsymbol{V}_1(p) \frac{A_R(p)}{B_R(p)} = -\boldsymbol{V}_1(p) \frac{L_m (p - j\omega)}{\sigma L_S L_R (p - p_1)(p - p_2)} \end{aligned} \tag{9}$$

In the foregoing equations, R_S is the stator resistance, R_R the rotor resistance, L_S the stator self-inductance, L_R the rotor self-inductance, L_m the mutual inductance and ω the rotor electrical angular velocity.

$$\sigma = 1 - \frac{L_m^2}{(L_S\ L_R)}, \quad k_S = \frac{R_S}{L_S}, \quad k_R = R_R / L_R$$

and $p_{1,2}$ in (9) are the roots of the characteristic equation: $B(p) = 0$, which are given as follows

$$p_{1,2} = \frac{-(k_S + k_R - j\sigma\omega)}{2\sigma} \pm \sqrt{\left(\frac{k_S + k_R - j\sigma\omega}{2\sigma}\right)^2 + \frac{j\omega k_S - k_S k_R}{\sigma}} \tag{10}$$

The inverse Laplace transform of (9) cannot be solved directly using the residue theorem, as (11) contains infinite numbers of poles given by the following equations (8)

$$\begin{aligned} & e^{j\pi/3} - e^{pT} = 0 \\ & e^{j(\pi/3 - 2\omega_1 T)} - e^{pT} = 0, \quad e^{j(\pi/3 + 2\omega_1 T)} - e^{pT} = 0 \end{aligned} \tag{11}$$

The solution of the time dependency of the motor current vectors can be found in the closed form as presented in [5].

If we use the Heasivide theorem

$$L^{-1}\left\{\frac{A(p)}{pB(p)}\right\} = \frac{A(0)}{B(0)} + \sum_k \frac{A(p_k)}{p_k \dot{B}(p_k)} e^{p_k T} \tag{12}$$

and also the formula for multiplication by an exponential function

$$L\{e^{j\omega T} f(t)\} = F(p - j\omega T) \tag{13}$$

where $\dot{B}(p_k) = (dB/dp)p = p_k$ and symbols $L\{\ \}$ and $L^{-1}\{\ \}$ mean the direct and inverse Laplace transforms, respectively, we can transform the formulas for the motor currents (9) from the Laplace into the modified Z-domain [8]. After doing that we can use the residue theorem in the modified Z-transform to find the analytical closed-form solution both for the stator and for the rotor current vectors. Details of this analysis and the corresponding coefficients are provided in Appendix and in [7]. The solution contains both the steady-state and transient components. As our attention is focused on the steady-state solution, applying superposition, the stator and rotor currents will have the closed-form solution shown in (14), for $n \to \infty$

$$\begin{aligned} I_y(n, \varepsilon) = {} & I_y^1(0) e^{j\pi/3(n+1)} + \sum_{k=1}^{2} I_y^1(p_k) e^{j\pi/3(n+1)} e^{p_k T\varepsilon} \\ & + I_y^2(2j\omega_1) e^{j\pi/3(n+1)} e^{2j\omega_1 T(n+\varepsilon)} \\ & + \sum_{k=1}^{2} I_y^2(p_k - 2j\omega_1) e^{j(\pi/3 + 2\omega_0 T)(n+1)} e^{p_k T\varepsilon} \\ & + I_y^3(-2j\omega_1) e^{j\pi/3(n+1)} e^{-2j\omega_1 T(n+\varepsilon)} \\ & + \sum_{k=1}^{2} I_y^3(p_k + 2j\omega_1) e^{j(\pi/3 - 2\omega_0 T)(n+1)} e^{p_k T\varepsilon} \\ = {} & I_{y0}(n, \varepsilon) + I_{yp}(n, \varepsilon) + I_{yn}(n, \varepsilon) \end{aligned} \tag{14}$$

where y is S (for the stator values) or y is R (for the rotor values), 0 are parts of (14) that are not dependent on angular frequency ω_1, p means a positive sequence terms (depending on ω_1) and n a negative sequence terms (depending on $-\omega_1$).

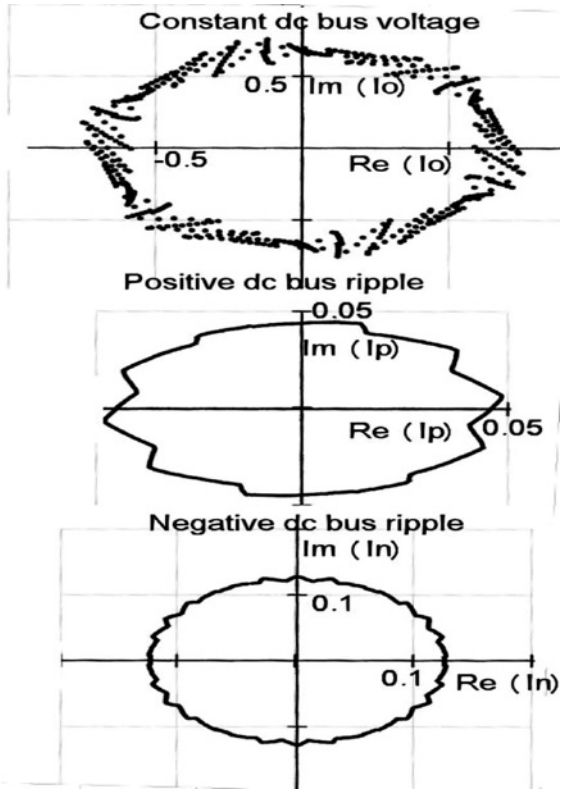

Figure 4 *Closed-form analysis results of machine stator current vectors*

$\Delta V_{DC} = 0.05$, $f_0 = f_1 = 50$ Hz, $f_{sw} = 3000$ Hz
Trajectories of the stator current vectors

Similar to (8), the overall steady-state stator/rotor currents contain three parts (terms arising from constant, positive and negative bus voltages, respectively).

These components are shown in Fig. 4 for the pulsation of the DC bus 5%. The upper plot in Fig. 4 shows the current space-vector trajectory from the constant DC bus voltage, the middle and bottom plots show, respectively, the current space-vector trajectory from the positive and negative DC bus voltage components. Fig. 5 shows the induction machine stator phase currents, again for $f_1 = f_0 = 50$ Hz, $f_{SW} = 3000$ Hz and the ac ripple voltage $\Delta\ V_{DC} = 0.05$. As it will be shown in the section concerning the frequency-domain analysis, the currents contain harmonics

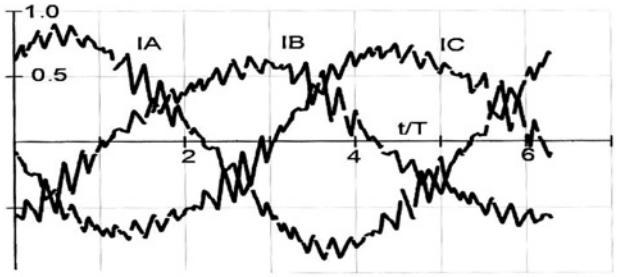

Figure 5 *Closed-form analysis results of machine phase currents*

$\Delta V_{DC} = 0.05$, $f_0 = f_1 = 50$ Hz, $f_{sw} = 3000$ Hz

with frequencies 150 Hz (positive-sequence third-harmonic component) and −50 Hz, (negative-sequence fundamental component), respectively. These harmonics cause the unbalance stator phase current waveforms as seen in Fig. 5.

Owing to the DC bus voltage pulsation, the phase currents are distorted.

3.2 Electromagnetic torque

Torque ripple with low frequency may become an important issue in induction motor drives. It causes mechanical oscillations, which are particularly dangerous in resonance frequencies of the system [11–13].

This torque ripple is usually superimposed to the torque ripple of switching frequency. Since the switching frequency usually has a high value, its effect will be suppressed by the electrical and mechanical damping of the motor and the gear.

In steady state, along with an expected torque ripple of switching frequency, a superimposed pulsation was observed. Particularly, the appearance of the sixth torque harmonic was observed by many researchers [7, 9].

As it was shown in [9], the occurrence of zero vector intervals in PWM influences torque ripple and leads to a sixth-order torque harmonics. But as it will be shown in the following part of this paper, the DC bus voltage pulsation with angular frequency $2\omega_1$ may cause large torque pulsation with the same angular frequency.

The electromagnetic torque is given from the stator and rotor vector current by the following formula

$$T_i(n, \varepsilon) = \frac{3}{2} L_m \frac{P}{2} \mathrm{Re}\{j \cdot I_s^*(n, \varepsilon) \cdot I_r(n, \varepsilon)\} \quad (15)$$

where symbol * means complex conjugate value and P is the number of poles.

The expression for the complex stator and rotor currents in (14) can be used to develop an expression for the product in (15) as follows

$$\begin{aligned} T_i(n, \varepsilon) &= \frac{3}{2} L_m \frac{P}{2} \mathrm{Re}\{j \cdot I_{S0}^*(n, \varepsilon) \cdot I_{R0}(n, \varepsilon)\} \\ &+ \frac{3}{2} L_m \frac{P}{2} \mathrm{Re}\{j(I_{Sp}^*(n, \varepsilon) + I_{Sn}^*(n, \varepsilon)) I_{R0}(n, \varepsilon)\} \\ &+ \frac{3}{2} L_m \frac{P}{2} \mathrm{Re}\{j I_{S0}^*(n, \varepsilon)(I_{Rp}(n, \varepsilon) + I_{Rn}(n, \varepsilon))\} \\ &+ \frac{3}{2} L_m \frac{P}{2} \mathrm{Re}\{j(I_{Sp}^*(n, \varepsilon) + I_{Sn}^*(n, \varepsilon))(I_{Rp}(n, \varepsilon) \\ &+ I_{Rn}(n, \varepsilon))\} \\ &= T_{i0}(n, \varepsilon) + T_{i1}(n, \varepsilon) + T_{i2}(n, \varepsilon) + T_{iC}(n, \varepsilon) \end{aligned} \quad (16)$$

doi: 10.1049/iet-epa:20070372

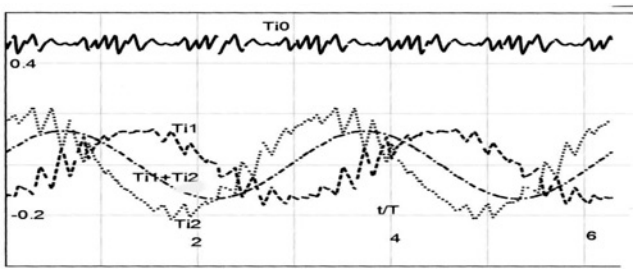

Figure 6 *Closed-form analysis results of electromagnetic torque and its components*

Solid line, overall pulsation torque [$T_{i\mathrm{PUL}}(n, \varepsilon)$]; dashed line, first pulsation component ($T_{i1}[n,\varepsilon)$], dotted line, second pulsation component [$T_{i2}(n, \varepsilon)$]; dash-dotted line, the overall pulsation component [$T_{i1}(n, \varepsilon)+ T_{i2}(n, \varepsilon)$], $f_0 = f_1 = 50$ Hz, $f_{\mathrm{SW}} = 3000$ Hz, $\Delta V_{\mathrm{DC}} = 0.05$

This expression shows that, under unbalance input voltage conditions, the electromagnetic torque contains the following terms: $T_{i0}(n, \varepsilon)$ is the electromagnetic torque without DC bus ripple component. It contains an average DC term and sixth-harmonic pulsations caused by the inverter switching frequency. $T_{i1}(n, \varepsilon)$ and $T_{i2}(n, \varepsilon)$ represent the products of the complex conjugate stator currents, which form the constant (ripple) DC bus and the complex rotor currents from the ripple (constant) DC bus voltage. $T_{i\mathrm{C}}(n, \varepsilon)$ is the electromagnetic torque component from stator and rotor DC link pulsation parts. It has negligible value and we may put $T_{i\mathrm{C}}(n, \varepsilon) = 0$. The separated torque components can be seen from Fig. 6.

From Fig. 6, we can see that the overall pulsating electromagnetic torque can be expressed as follows

$$\begin{aligned} T_{i\mathrm{PUL}}(n, \varepsilon) &= T_{i1}(n, \varepsilon) + T_{i2}(n, \varepsilon) \\ &= A_{\mathrm{T}} \cdot \sin(2 \cdot \omega_0 \cdot (n + \varepsilon)\mathrm{T} + \psi)) \end{aligned} \tag{17}$$

where A_{T} is an amplitude of the pulsating torque component (in Fig. 6, we have $A_{\mathrm{T}} = 0.073$ p-u.) and ψ is a phase angle (in Fig. 6, we have $\psi = 8.3^{\circ}$).

As can be seen from Fig. 6, both electromagnetic components forming the pulsation part have opposite direction and their sum is the pulsating waveform with the sine time dependency (without any high-frequency ripple). The frequency of the pulsation is given by the frequency of the DC bus voltage pulsation $2\omega_1$.

3.3 Frequency-domain analysis

We shall calculate the Fourier series of the periodic variation of the stator voltage space vector

$$V(n, \varepsilon) = \sum_{k=-k_{\max}}^{k_{\max}} C_k \mathrm{e}^{jk\omega_0 T(n+\varepsilon)} \tag{18}$$

$k_{\min}$ and $k_{\max}$ are the upper and lower limits, respectively, for the Fourier series expansion.

Using superposition of the two parts of the DC bus voltage (constant and pulsation parts) and (4), we can modify (18) as

$$\begin{aligned} V(n, \varepsilon) = &\sum_{k=-k_{\max}}^{k_{\max}} C_k^1 \mathrm{e}^{jk\omega_0 T(n+\varepsilon)} + \sum_{k=-k_{\max}}^{k_{\max}} C_k^2 \mathrm{e}^{jk\omega_0 T(n+\varepsilon)} \\ &\times (\mathrm{e}^{j2\omega_1 T(n+\varepsilon)} + \mathrm{e}^{-2j\omega_1 T(n+\varepsilon)}) \end{aligned} \tag{19}$$

where C_k^1 and C_k^2 are, respectively, the Fourier coefficients for DC smooth and pulsation parts.

To derive the coefficients of the Fourier analysis, we can use the relation between the Laplace transform of the periodic waveform and Fourier coefficients

$$C_\mu = \left[\frac{1}{T_1}(1 - (\exp(-pT_0))V(p)\right]_{p=\mathrm{j}\mu\omega_0} \tag{20}$$

Substituting into (20) from first part of (8), for the Fourier coefficients of the constant DC bus voltage we have,

$$\begin{aligned} C_\mu^1 = &\frac{2V_{DC}}{3}\frac{1}{\pi j\mu}\frac{[\exp(j\mu\pi/3) - \exp(-5j\mu\pi/3)]}{[\exp(j\mu\pi/3) - \exp(j\pi/3)]} \\ &\times \sum_k \exp\left[\frac{j\pi\alpha_k}{3}\right]\left[\exp\left(-jl\frac{\pi}{3}\varepsilon_{\mathrm{A}k}\right) - \exp\left(-jl\frac{\pi}{3}\varepsilon_{Bk}\right)\right] \end{aligned} \tag{21}$$

Equation (21) has a non-zero value only for harmonics order

$$\mu = 1 + 6\nu, \quad \nu = 0, \pm 1, \pm 2, \ldots. \tag{22}$$

By substituting (22) into (21), the Fourier coefficients are

$$\begin{aligned} C_\nu^1 = &\frac{2V_{DC}}{3\pi j(1+6\nu)}\sum_k \exp j\pi\frac{\alpha_k}{3} \\ &\times \left[\exp\left(-j(1+6\nu)\frac{\pi}{3}\varepsilon_{\mathrm{A}k}\right) - \exp\left(-j(1+6\nu)\frac{\pi}{3}\varepsilon_{\mathrm{B}k}\right)\right] \end{aligned} \tag{23}$$

Similarly, we can derive for the second part of (8)

$$\begin{aligned} C_\nu^2 = &\frac{\Delta V_{DC}}{3\pi j(1+6\nu)}\sum_k \exp \mathrm{j}\pi\frac{\alpha_k}{3}\left[\exp\left(-\mathrm{j}(1+6\nu)\frac{\pi}{3}\varepsilon_{\mathrm{A}k}\right)\right. \\ &\left. - \exp\left(-\mathrm{j}(1+6\nu)\frac{\pi}{3}\varepsilon_{\mathrm{B}k}\right)\right] = \frac{C_\nu^1}{V_{DC}}\frac{\Delta V_{DC}}{2} \end{aligned} \tag{24}$$

The Fourier series expansion of the overall voltage space vector will have the following form

$$\begin{aligned} V(n, \varepsilon) = &\sum_{\nu=-\nu_{\max}}^{\nu_{\max}} C_\nu^1 \mathrm{e}^{j(1+6\nu)\omega_0 T(n+\varepsilon)} + \sum_{\nu=-\nu_{\max}}^{\nu_{\max}} \\ &\times C_\nu^1 \frac{\Delta V_{DC}}{2V_{DC}} \mathrm{e}^{j(1+6\nu)\omega_0 T(n+\varepsilon)} \mathrm{e}^{2j\omega_1(n+\varepsilon)T} \\ &+ \sum_{\nu=-\nu_{\max}}^{\nu_{\max}} C_\nu^1 \frac{\Delta V_{DC}}{2V_{DC}} \mathrm{e}^{j(1+6\nu)\omega_0 T(n+\varepsilon)} \mathrm{e}^{-2j\omega_1(n+\varepsilon)T} \end{aligned} \tag{25}$$

From (25), it may be seen that harmonic spectrum contains harmonics with frequencies $(1+6\nu)f_1$ and amplitudes C_ν^1 as in VSI without DC bus pulsations and also harmonics with the sum and difference frequencies $(1+6\nu)f_1+2f_0$ and $(1+6\nu)f_1-2f_0$, respectively, both with reduced harmonic amplitudes

$$1 = C_\nu^1 \frac{\Delta V_{DC}}{2V_{DC}}$$

For example, if $f_0 = f_1 = 50$ Hz, we have harmonics

$$(1+6\nu)50 \text{ Hz}, \quad (1+6\nu)50+100 \text{ Hz}, \quad (1+6\nu)50-100 \text{ Hz}$$

It means that for $\nu = 0$ (the fundamental harmonic), we have harmonics with frequencies 50, 150 and -50 Hz, for $\nu = 1$ (the seventh harmonic), we have harmonics with frequencies 350, 450 and 250 Hz, for $\nu = -1$ (the fifth harmonic), we have frequencies -250, -150 and -350 Hz and so on.

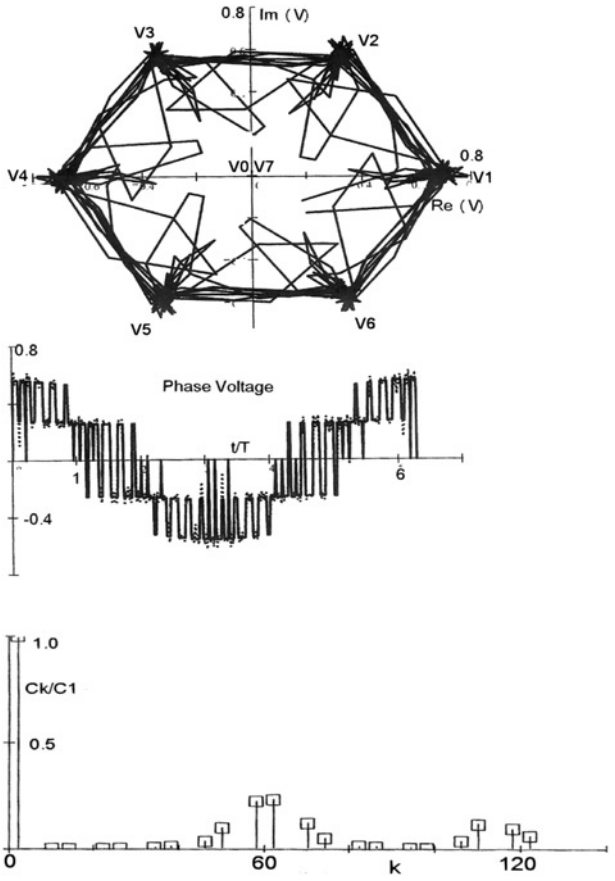

Figure 7 *Fourier series expansion of the voltage space-vector (upper trace) and its phase-voltage waveform (middle trace)*
Theoretical harmonic spectrum (bottom trace)
$f_0 = f_1 = 50$ Hz, $f_{sw} = 3000$ Hz, $\Delta V_{DC} = 0.05$, $k_{max} = 30$

The Fourier series approximation of the voltage space-vector trajectory is shown in the upper plot in Fig. 7. It is calculated from (23) to (25) for SVPWM, if we consider number of harmonics $\nu_{min} = \nu_{max} = 30$. This trajectory can be compared with the theoretical one shown in Fig. 2. Again, we can see the position of the six non-zero voltage space vectors $\boldsymbol{V}_1$–$\boldsymbol{V}_6$ and the zero voltage vectors $\boldsymbol{V}_0$ and $\boldsymbol{V}_7$. Also, we can see the influence of the DC link voltage pulsation.The Fourier series approximation can be done both for the space vectors and the phase voltages.

The phase voltage approximation can be calculated as a real part of (25) and is shown in the middle plot of Fig. 7 (dotted line). As can be seen by comparing with the theoretical voltage waveform (solid line), the correlation is high.

The harmonic spectrum $C_\nu^1/C_{\nu=0}^1$ given from (23) is shown in the bottom part in Fig. 7. The harmonic

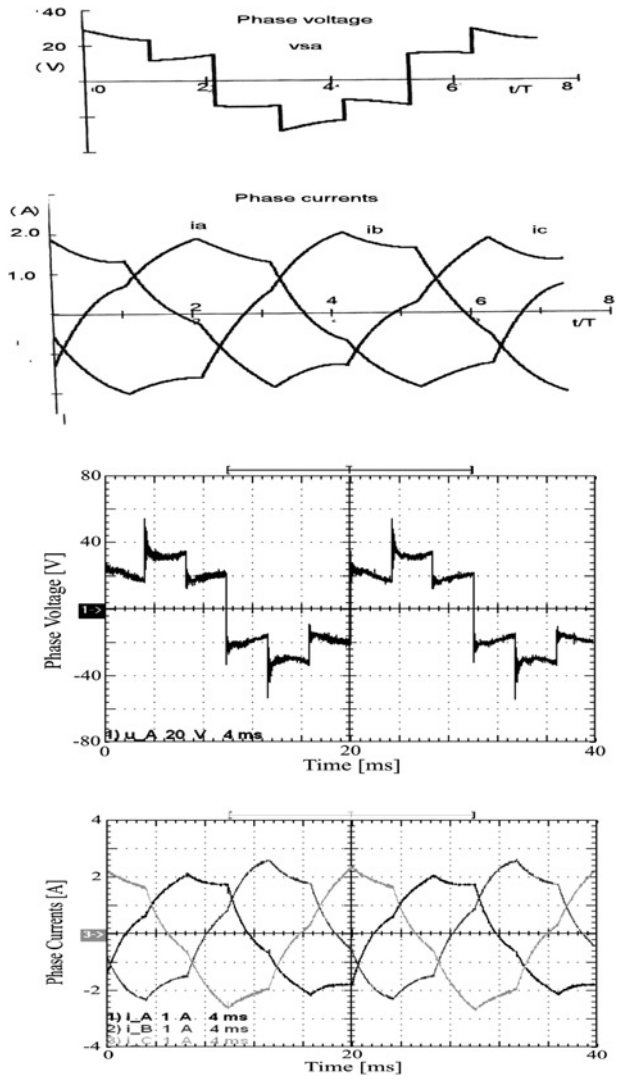

Figure 8 *Closed-form analytical results (upper traces) and measured (bottom traces) stator-current and stator-voltage waveforms with DC bus voltage ripple $\Delta V_{DC} = 0.05$, slip $s = 0.6$*

IET Electr. Power Appl., 2008, Vol. 2, No. 6, pp. 341–352
doi: 10.1049/iet-epa:20070372

spectrum is calculated for switching frequency 3000 Hz and modulation factor $m_{id} = 1$. The harmonic spectrum is typical for synchronous SVPWM.

4 Experimental verification

The analytical results and experimental waveforms for the sake of comparison are presented. All the analytical results were visualised from the derived equations by the program MATHCAD.

Experimental tests have been carried out using the motor with the following parameters: (1.1 kW, 50 Hz, d/y 230 V/400 V, 4.2 A/2.4 A, cos φ = 0.87, 2845 rpm. The motor was mounted on a laboratory AC dynamometer. The capacity in the DC bus was 900 μF (2 × 1800 μF/400 V capacitors in series). In order to conveniently simulate the operation of the VSI under the condition of pulsating DC link voltage, an experimental setup has been built. The DC link voltage was composed of two separate voltage components. The constant DC voltage was supplied by a three-phase diode rectifier charging a large capacitor bank in the DC bus. The voltage ripple was superimposed to this DC voltage by means of a variable transformer supplied by an auxiliary VSI producing a PWM voltage waveform with the fundamental frequency of 100 Hz. Some filtering components were added to the circuit in order to obtain smoother waveforms at the input of the output stage of the main inverter. This output stage generated either a six-pulse or an SVPWM voltage output feeding an induction machine mechanically loaded by a dynamometer.

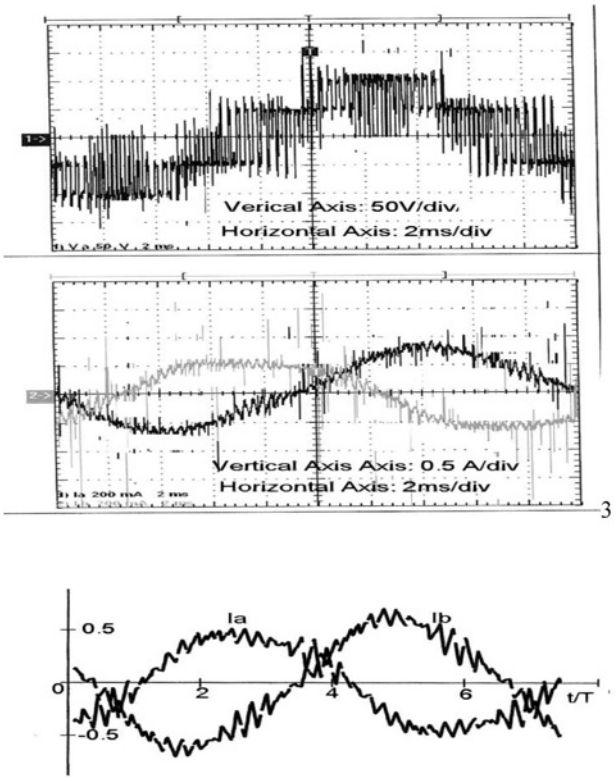

Figure 9 *Measured phase voltage (upper trace), measured stator phase current (middle trace) and closed-form analytical results bottom trace) of machine stator phase currents with 5% AC link voltage ripple, slip s = 0.015*

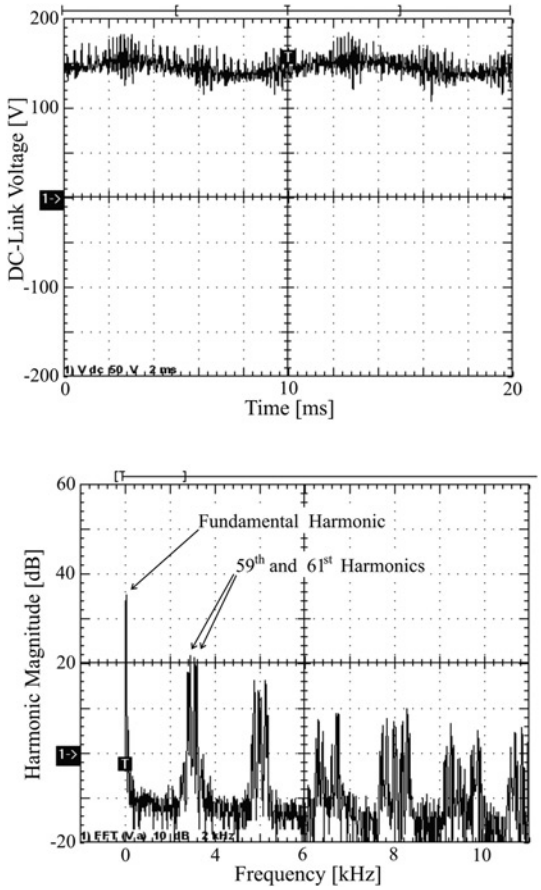

Figure 10 *Measured DC bus voltage $V_{DC}(t)$ with $\Delta V_{DC} = 0.05$ (upper trace)*
Measured phase voltage harmonic spectrum (bottom trace)

First, the comparison is made for the case of square-waveforms (without modulation), as in this case we can see the most pronounced influence of the DC link voltage ripple. The current waveforms in Fig. 8 for 5% DC link voltage ripple and slip $s = 0.6$ show the same features both for the experiments and closed-form analytical results. From top to bottom, we can see:

(i) analytical calculated phase voltage,

(ii) analytical calculated phase currents,

(iii) measured phase voltage and

(iv) measured phase currents.

The next comparison is made for the SVPPMW waveforms.

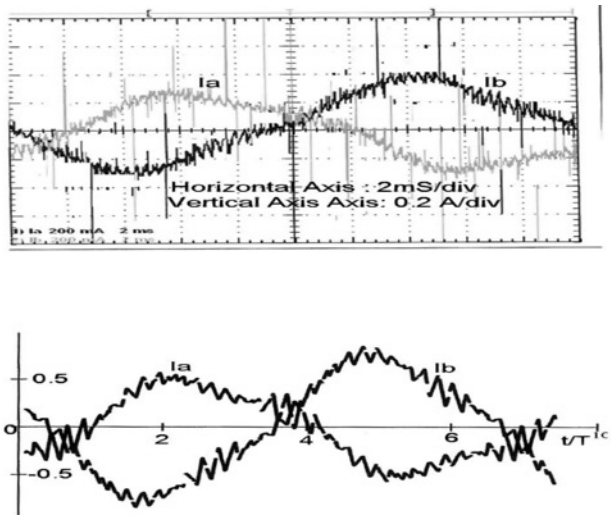

Figure 11 *Measured (upper trace) stator-current waveforms with* $\Delta V_{DC} = 0.1$
Closed-form (bottom trace) calculated stator-current waveforms

Fig. 9 shows the measurement (upper and middle traces) and analytical calculated (bottom trace) results of the stator voltage and current waveforms for 5% pulsation with 4% motor slip.

The upper plot in Fig. 10 shows the DC link voltage with the dominant AC frequency 100 Hz. The lower plot in Fig. 10 shows the phase voltage spectrum with 5% AC voltage ripple component. The measured spectrum is in good correlation with that calculated analytically and is shown in Fig. 7.

The measurement and analytical calculated phase current waveforms for higher value of the AC pulsation (10%) and slip s = 4 % are shown in Fig. 11. The measured current waveforms in Fig. 11 show the same features as that for the calculated current waveform, including a high switching frequency ripple, providing further confirmation of the closed-form analytical results.

5 Conclusion

Analytical analysis and mathematical closed-form model of three-phase voltage source PWM inverter fed induction motor drive under the DC link ripple voltage component are presented in this paper. The analytical expressions for the voltage and current space vectors as a function of the DC-link voltage pulsation are derived. By means of the modified Z-transform and the mixed p–z approach, we can estimate the separate parts of the solution to estimate the influence of the DC link voltage pulsating on the current and torque waveforms.

The availability of the closed-form solution makes it possible to rapidly calculate the impact of the input unbalance conditions on the operating performance of an induction motor supplied from SVPWM VSI with finite value of DC bus capacitance. Torque ripple produced in PWM-inverter-fed induction motor drives deteriorates both the steady-state and dynamic characteristics. It was found that the DC- link ripple voltage components with angular frequency ω_0 may cause large torque pulsation with the same angular frequency. This torque ripple may be even dangerous at resonance frequencies of the system.

6 Acknowledgment

This work was supported by the Czech Grant Agency (GACR) under the contract 102/08/0424.

7 References

[1] LEE K., JAHNS T.M., BERKOPEC W.E., LIPO T.A.: 'Closed-form analysis of adjustable-speed drive performance under input-voltage unbalance and sag conditions', *IEEE Trans. Ind. Appl.*, 2006, **42**, (3), pp. 733–741

[2] BROECK H.W., SKUDELNY H.-C.: 'Analytical analysis of the harmonic effects of a PWM AC drive', *IEEE Trans. Power Electron.*, 1988, **3**, (2), pp. 216–222

[3] ANDRESEN E.C., HAUNT A.: 'Influence of the pulsewidth modulation control method on the performance of frequency inverter induction motor drives', *Eur. Trans. Electr. Power*, 1993, **3**, pp. 151–161

[4] DE ABREU J.P.G., EMANUEL A.E.: 'Induction motor thermal aging caused by voltage distortion and unbalance: loss of useful life and its estimated cost', *IEEE Trans. Ind. Appl.*, 2000, **38**, (1), pp. 12–20

[5] CHOMAT M., SCHREIER L.: 'Compensation of unbalanced three-phase voltage supply in voltage source inverter'. Proc. 28th Annual Conf. IEEE Industrial Society, 2002, pp. 950–955

[6] MORAN L., ZIOGAS S.P., JOOS G.: 'Design aspects of synchronous PWM rectifier-inverter systems under unbalanced input voltage conditions', *IEEE Trans. Ind. Appl.*, 1992, **28**, (6), pp. 1286–1293

[7] KLIMA J.: 'Analytical closed-form solution of a space-vector modulated VSI feeding an induction motor drive', *IEEE Trans. Energy Conversion*, 2002, **17**, (2), pp. 191–196

[8] KLIMA J.: 'Mixed p-z approach for time-domain analysis of voltage source inverters with periodic pulse width modulation', *IEEE Trans. Circuits Syst., II*, 2004, **51**, (10), pp. 529–536

[9] HOLTZ J.: 'Identification and compensation of torque ripple in high-precision permanent magnet motor drives', *IEEE Trans. Ind. Electron.*, 1996, **43**, (2), pp. 309–320

doi: 10.1049/iet-epa:20070372

[10] HOFMAYER F.: 'Harmonic torque pulsation of induction machines-Analysis and compensation techniques using PWM inverters'. Proc. EPE Conf., Toulose, France, 2003, pp. 247–251

[11] CROSS A.M., EVANS P.D.: 'DC link current in PWM inverters with unbalanced and non-linear loads', *IEE Proc. Electr.Power. Appl.*, 1999, **43**, (6), pp. 620–626

[12] CHOMAT M., SCHREIER L.: 'Control method for DC-link voltage ripple cancellation in voltage source inverter under unbalanced three-phase voltage supply conditions', *IEE Proc. Electr. Power Appl.*, 2005, **152**, (3), pp. 494–500

[13] BROECK H.W., WYK J.D.: 'A Comparative investigation of a three-phase induction machine drive with a component minimised voltage-fed inverter under different control options', *IEEE Trans. Ind. Appl.*, 1984, **20**, pp. 309–320

8 Appendix

8.1 Closed-form derivation

Using (2) and (3), the Laplace transform of the load current can be expressed as

$$\begin{aligned} I_y(p) = V_1(p)\frac{A_y(p)}{B_y(p)} &= \frac{2}{3}V_{DC}\frac{1}{p}\frac{e^{pT}}{e^{pT}-e^{j\pi/3}} \\ &\times \sum_k (e^{-pT\varepsilon_{kA}} - e^{-pT\varepsilon_{kB}})\frac{A_y(p)}{B_y(p)} \\ &+ \frac{1}{3}\Delta V_{DC}\frac{1}{p-2j\omega_1}\frac{e^{pT}}{e^{pT}-e^{j(\pi/3+2\omega_1 T)}} \\ &\times \sum_k (e^{-T\varepsilon_{kA}(p-2j\omega_0)} - e^{-T\varepsilon_{kB}(p-2j\omega_0)})\frac{A_y(p)}{B_y(p)} \\ &+ \frac{1}{3}\Delta V_{DC}\frac{1}{p+2j\omega_1}\frac{e^{pT}}{e^{pT}-e^{j(\pi/3-2\omega_1 T)}} \\ &\times \sum_k (e^{-T\varepsilon_{kA}(p+2j\omega_0)} - e^{-T\varepsilon_{kB}(p+2j\omega_0)})\frac{A_y(p)}{B_y(p)} \\ &= R_1(e^{pT})Q_1(p) + R_2(e^{pT})Q_2(p) + R_3(e^{pT})Q_3(p) \end{aligned} \quad (26)$$

where the polynomials are defined as follows:

$$\begin{aligned} R_1(e^{pT}) &= \frac{e^{pT}}{e^{pT}-e^{j\pi/3}} \\ R_2(e^{pT}) &= \frac{e^{pT}}{e^{pT}-e^{j(\pi/3+2\omega_1 T)}} \\ R_3(e^{pT}) &= \frac{e^{pT}}{e^{pT}-e^{j(\pi/3-2\omega_1 T)}} \end{aligned} \quad (27)$$

$$\begin{aligned} Q_1(p) &= \frac{2}{3}V_{DC}\frac{1}{p}\sum_k (e^{-pT\varepsilon_{kA}} - e^{-pT\varepsilon_{kB}})\frac{A_y(p)}{B_y(p)} \\ Q_2(p) &= \frac{1}{3}\Delta V_{DC}\frac{1}{p-2j\omega_1} \\ &\times \sum_k (e^{-T\varepsilon_{kA}(p-2j\omega_0)} - e^{-T\varepsilon_{kB}(p-2j\omega_0)})\frac{A_y(p)}{B_y(p)} \\ Q_3(p) &= \frac{1}{3}\Delta V_{DC}\frac{1}{p+2j\omega_1} \\ &\times \sum_k (e^{-T\varepsilon_{kA}(p+2j\omega_0)} - e^{-T\varepsilon_{kB}(p+2j\omega_0)})\frac{A_y(p)}{B_y(p)} \end{aligned} \quad (28)$$

As can be seen from (26), the Laplace transform of the motor current consists of three terms, each with two multiplicative parts. One $[R(e^{pT})]$ is a function of e^{pT} operator, the other $[Q(p)]$ is a function of p-operator. To find the original function of (26), we can use the residual theorem.

But the inverse transform of (26) cannot be carried out in a direct way as it contains infinite number of poles given by

$$\begin{aligned} &e^{pT} - e^{j\pi/3} = 0, \quad e^{pT} - e^{j(\pi/3+2j\omega_1 T)} = 0 \\ &e^{pT} - e^{j(\pi/3-2j\omega_1 T)} = 0 \end{aligned} \quad (29)$$

From (26), it may be seen that using superposition each term can be separated into two multiple parts and so we can transform it into the modified Z-transform [7]. In doing so, in the modified Z-space, we obtain

$$\begin{aligned} I_y(z, \varepsilon) = R_1(z)\cdot Z_m\{Q_1(p)\} + R_2(z)\cdot Z_m\{Q_2(p)\} + R_3(z) \\ \cdot Z_m\{Q_3(p)\} \end{aligned} \quad (30)$$

with $Z_m\{\}$ denotes the modified Z-transform operator.

In order to find Z-transform of $Q_i(p)$, we must use the translation theorem in Z-transform which holds

$$Z_m\{e^{-p.a}\cdot F(p)\} = z^{-x}\cdot F(z, \varepsilon - a + x) \quad (31)$$

where the parameter x is given by

$$x = \begin{cases} 1 & \text{for} \quad 0 \le \varepsilon < a \\ 0 & \text{for} \quad a \le \varepsilon < 1 \end{cases} \quad (32)$$

If we want to express translation for kth pulse, with the beginning ε_{kA} and the end ε_{kB}, (pulse width $\Delta\varepsilon_k = \varepsilon_{kB} - \varepsilon_{kA}$), we can use two parameters, namely M_k and L_k to determine the per-unit time for pre-pulse, inside-pulse and post-pulse switching times, respectively.

M_k is a parameter that defines the beginning of the kth pulse ε_{kA}, L_k is a parameter that defines the end of the kth pulse ε_{kB}According to (32), we can write for M_k and L_k,

respectively

$$M_k=\begin{cases}1 & \text{for} \quad 0\le\varepsilon\le\varepsilon_{k\mathrm{A}}\\ 0 & \text{for} \quad \varepsilon_{k\mathrm{A}}\le\varepsilon\le 1\end{cases} \quad L_k\begin{cases}1 & \text{for} \quad 0\le\varepsilon\le\varepsilon_{k\mathrm{B}}\\ 0 & \text{for} \quad \varepsilon_{k\mathrm{B}}\le\varepsilon\le 1\end{cases} \tag{33}$$

By means of these two parameters, we can express per unit time for the three intervals:

(a) $0<\varepsilon\le\varepsilon_{k\mathrm{A}}$ prepulse per unit time. $M_k=1,\ L_k=1$

(b) $\varepsilon_{k\mathrm{A}}<\varepsilon\le\varepsilon_{k\mathrm{B}}$ inside pulse per unit time $M_k=0,$ $L_k=1$ (34)

(c) $\varepsilon_{k\mathrm{B}}<\varepsilon\le 1$ post-pulse per unit time $M_k=0,\ L_k=0$

Thus, in a period nT, for per unit time $0<\varepsilon\le 1$, we obtain from (33) for per unit time $0<\varepsilon\le 1$ two parameters M_k and L_k, which will be used for solution of (28) in the modified Z-transform.

Using parameters M_k, L_k and Heaviside theorem (12), we can express the first part of (26) with help of (33) in the modified Z-space as follows:

$$\begin{aligned}I_{\mathrm{y}}^1(z,\varepsilon)=&\frac{2V_{\mathrm{DC}}}{3}\frac{z}{z-\mathrm{e}^{j(\pi/3)}}\\&\times\sum_k\left\{\frac{A_{\mathrm{y}}(0)}{B_{\mathrm{y}}(0)}\mathrm{e}^{j\pi\alpha_k/3}\frac{z}{z-1}(z^{-M_k}-z^{-L_k})\right.\\&+\sum_{s=1}^{2}\frac{A_{\mathrm{y}}(p_s)}{p_sB_{\mathrm{y}}(p_s)}e^{j\pi\alpha_k/3}\frac{z\mathrm{e}^{p_sT\varepsilon}}{z-\mathrm{e}^{p_sT}}\\&\left.\times\left[z^{-M_k}\mathrm{e}^{p_sT(M_k-\varepsilon_{k\mathrm{A}})}-z^{-L_k}\mathrm{e}^{p_sT(L_k-\varepsilon_{k\mathrm{B}})}\right]\right\}\end{aligned} \tag{35}$$

Equation (35) has simple poles $\mathrm{e}^{\mathrm{j}(\pi/3)}$, 1, e^{p_sT}. The inverse Z-transform of (35) can be found using an integral

$$I^1(n,\varepsilon)=\frac{1}{2\pi j}\oint I^1(z,\varepsilon)z^{n-1}\mathrm{d}z \tag{36}$$

Integral (36) may be solved by means of the residual theorem. As our attention is paid to the steady-state components, we obtain for $n\to\infty$, the following expression

$$\begin{aligned}I_y^1(n,\varepsilon)=&\frac{2V_{\mathrm{DC}}}{3}\sum_k\left\{\frac{A_{\mathrm{y}}(0)}{\mathrm{B_y}(0)}\mathrm{e}^{j\pi\alpha_{\mathrm{k}}/3}\mathrm{e}^{j\pi(n+1)/3}\right.\\&\times\frac{(\mathrm{e}^{-j(\pi/3)M_k}-\mathrm{e}^{-j(\pi/3)L_k})}{(\mathrm{e}^{j(\pi/3)}-1)}+\sum_{s=1}^{2}\frac{A_{\mathrm{y}}(p_s)}{p_{\mathrm{s}}B_{\mathrm{y}}(p_s)}\mathrm{e}^{j\pi\alpha_{\mathrm{k}}/3}\\&\times\frac{\mathrm{e}^{j(\pi/3)(n+1)}}{(\mathrm{e}^{j(\pi/3)}-\mathrm{e}^{p_sT})}\mathrm{e}^{p_sT\varepsilon}\left[\mathrm{e}^{-j(\pi/3)M_k+p_sT(M_k-\varepsilon_{k\mathrm{A}})}\right.\\&\left.\left.-\mathrm{e}^{-j(\pi/3)L_{\mathrm{k}}+p_sT(L_k-\varepsilon_{k\mathrm{B}})}\right]\right\}\\=&I_{\mathrm{y}}^1(0)\mathrm{e}^{j\pi/3(n+1)}+\sum_{s=1}^{2}I_{\mathrm{y}}^1(p_s)\mathrm{e}^{j\pi/3(n+1)}\mathrm{e}^{p_sT\varepsilon}\end{aligned}$$

where

$$\begin{aligned}I_{\mathrm{y}}^1(0)=&\frac{2V_{\mathrm{DC}}}{3}\sum_{\mathrm{k}}\left\{\frac{A_{\mathrm{y}}(0)}{B_{\mathrm{y}}(0)}\mathrm{e}^{j\pi\alpha_{\mathrm{k}}/3}\frac{(\mathrm{e}^{-j(\pi/3)M_k}-\mathrm{e}^{-j(\pi/3)L_k})}{(\mathrm{e}^{j(\pi/3)}-1)}\right\}\\I_{\mathrm{y}}^1(p_s)=&\frac{2V_{\mathrm{DC}}}{3}\sum_k\sum_{s=1}^{2}\frac{A_{\mathrm{y}}(p_s)}{p_sB_{\mathrm{y}}(p_{\mathrm{s}})}\frac{\mathrm{e}^{j\pi\alpha_{\mathrm{k}}/3}}{(\mathrm{e}^{j(\pi/3)}-\mathrm{e}^{p_sT})}\\&\times\left[\mathrm{e}^{-j(\pi/3)M_k+p_sT(M_k-\varepsilon_{k\mathrm{A}})}-\mathrm{e}^{-j(\pi/3)L_{\mathrm{k}}+p_sT(L_k-\varepsilon_{k\mathrm{B}})}\right]\end{aligned} \tag{37}$$

Equation (37) is the time dependency of the first part of the current space vector in the stator co-ordinate system. By the same way and by using the theorem for multiplication by an exponential function (13), we can derive the overall solution given in (14). The corresponding coefficients are given in (38) and (39)

$$\begin{aligned}I_{\mathrm{y}}^2=&\sum_{s=1}^{2}\frac{\Delta V_{\mathrm{DC}}}{3}\frac{A_s(2j\omega_1)}{B_s(2j\omega_1)}\sum_k\left[\frac{(\mathrm{e}^{-j(\pi/3)M_k}-\mathrm{e}^{-j(\pi/3)L_k})}{(\mathrm{e}^{j(\pi/3)}-1)}\mathrm{e}^{j(\pi/3)\alpha_k}\right]\\&+\sum_{s=1}^{2}\frac{\Delta V_{\mathrm{DC}}}{3}\frac{A_s(p_s)}{(p_s-2j\omega_1)B_s(p_s)}\\&\times\sum_k\left[\frac{(\mathrm{e}^{-j(\pi/3)M_k-2j\omega_1T(M_k-\varepsilon_{Ak})+p_sT(M_k-\varepsilon_{Ak})}\right.\\&\left.\frac{-\mathrm{e}^{-j(\pi/3)L_k-2j\omega_1T(L_k-\varepsilon_{Bk})+p_sT(L_k-\varepsilon_{Bk})})}{(\mathrm{e}^{j(\pi/3)+2j\omega_1T)}-\mathrm{e}^{p_sT})}\mathrm{e}^{j(\pi/3)\alpha_k}\right]\\=&I_{\mathrm{y}}^2(2j\omega_1)+I_{\mathrm{y}}^2(p_s-2j\omega_1)\end{aligned} \tag{38}$$

$$\begin{aligned}I_{\mathrm{y}}^3=&\sum_{s=1}^{2}\frac{\Delta V_{\mathrm{DC}}}{3}\frac{A_s(-2j\omega_1)}{B_s(-2j\omega_1)}\\&\times\sum_k\left[\frac{(\mathrm{e}^{-j(\pi/3)M_k}-\mathrm{e}^{-j(\pi/3)L_k})}{(\mathrm{e}^{j(\pi/3)}-1)}\mathrm{e}^{j(\pi/3)\alpha_k}\right]\\&+\sum_{s=1}^{2}\frac{\Delta V_{\mathrm{DC}}}{3}\frac{A_s(p_s)}{(p_s+2j\omega_1)B_s'(p_s)}\\&\times\sum_k\left[\frac{(\mathrm{e}^{-j(\pi/3)M_k-2j\omega_1T(M_k-\varepsilon_{Ak})+p_sT(M_k-\varepsilon_{Ak})}\right.\\&\left.\frac{-\mathrm{e}^{-j(\pi/3)L_k-2j\omega_1T(L_k-\varepsilon_{Bk})+p_sT(L_k-\varepsilon_{Bk})})}{(\mathrm{e}^{j(\pi/3)+2j\omega_1T)}-\mathrm{e}^{p_sT})}\mathrm{e}^{j(\pi/3)\alpha_k}\right]\\=&I_y^3(-2j\omega_0)+I_y^3(p_s+2j\omega_0)\end{aligned} \tag{39}$$

Provided that an assumption of constant rotor speed is made, it can be seen that the solution (37) is in closed form. For concrete solution, we must substitute in (35) only parameters of the load $[A(p),B(p)]$ and parameters of the inverter (V_{DC}, $\varepsilon_{k\mathrm{A}}$, $\varepsilon_{k\mathrm{B}}$, α_k).

The induction motor used for both the analytical and experimental investigation was rated at 400/230 V, 1.1 kW and 1430 rpm. Its per unit parameters are $R_{\mathrm{S}}=0.068$, $R_{\mathrm{R}}=0.07$, $L_{\mathrm{S}}=L_{\mathrm{R}}=1.39$ and $L_{\mathrm{m}}=1.382$.

doi: 10.1049/iet-epa:20070372